doi.org/10.1002/hlca.202300072

RESEARCH ARTICLE

HELVETICA chimica acta

Eutectic Molten Salt Synthesis of Highly Microporous Macrocyclic Porous Organic Polymers for CO_2 Capture

Timur Ashirov,[a] Thamon Puangsamlee,[b] Alexandra Robles,[b] Patrick W. Fritz,[a] Krzysztof Piech,[a] Ognjen Š. Miljanić,*[b] and Ali Coskun*[a]

[a] Department of Chemistry, University of Fribourg, Chemin du Musée 9, CH-1700 Fribourg, Switzerland, e-mail: ali.coskun@unifr.ch

[b] Department of Chemistry, University of Houston, 3585 Cullen Boulevard #112, Houston, TX 77204-5003, United States, e-mail: miljanic@uh.edu

Dedicated to *Scott Denmark* on the occasion of his 70th birthday

The development of porous materials is of great interest for the capture of CO_2 from various emission sources, which is essential to mitigate its detrimental environmental impact. In this direction, porous organic polymers (POPs) have emerged as prime candidates owing to their structural tunability, physiochemical stability and high surface areas. In an effort to transfer an intrinsic property of a cyclotetrabenzoin-derived macrocycle – its high CO_2 affinity – into porous networks, herein we report the synthesis of three-dimensional (3D) macrocycle-based POPs through the polycondensation of an octaketone macrocycle with phenazine-2,3,7,8-tetraamine hydrochloride. This polycondensation was performed under ionothermal conditions, using a eutectic salt mixture in the temperature range of 200 to 300 °C. The resulting polymers, named 3D-mmPOPs, showed reaction temperature-dependent surface areas and gas uptake properties. 3D-mmPOP-250 synthesized at 250 °C exhibited a surface area of 752 $m^2 g^{-1}$ and high microporosity originating from the macrocyclic units, thus resulting in an excellent CO_2 binding enthalpy of 40.6 kJ mol^{-1} and CO_2 uptake capacity of 3.51 mmol g^{-1} at 273 K, 1.1 bar.

Keywords: carbon dioxide capture, cyclotetrabenzoin, macrocycles, macrocyclic microporous porous organic polymers, molten salt synthesis, polymers, porous organic polymers.

Introduction

Anthropogenic emissions have significantly increased the atmospheric carbon dioxide (CO_2) level, which has now exceeded 418 ppm,[1] resulting in global warming, climate change and ocean acidification. To decrease CO_2 emissions from large point sources, amine-scrubbing using aqueous solutions of alkyl amines has been conventionally applied. While this approach offers high selectivity and low cost, the low uptake capacity, high energy penalty for regeneration, and the degradation and corrosive nature of amines present important challenges. Porous materials have emerged as potential alternatives owing to their high surface areas and tailor-made properties for high CO_2 affinity.[2] Porous organic polymers (POPs) are a promising class of porous materials owing their high porosity, structural tunability, excellent chemical and thermal stability.[3,4] The introduction of heteroatoms, such as N, O, or S can enhance CO_2 affinity through quadrupole-quadrupole interactions and have been employed as a general strategy.[5] Therefore, amines,[5] imines,[6] pyrazines,[7] nitriles,[8,9] cyanurates[10] and other nitrogen-rich functional groups[11,12] have been introduced either into the structures of monomers or through post-synthetic modification. Moreover, the

Supporting information for this article is available on the WWW under https://doi.org/10.1002/hlca.202300072

abundance of micropores (< 2 nm) and ultramicropores (< 0.7 nm) is another essential factor to increase CO_2 affinity owing to the interaction of CO_2 with multiple binding sites.[13] We recently summarized[3] the most critical parameters determining the CO_2 capture capacity for POPs, which also highlights the incorporation of shape-persistent macrocycles and cages,[14] that can host guest molecules *i.e.*, CO_2 and optimize the pore size and geometry for high CO_2 affinity into POPs.[7,15,16] The introduction of various macrocycles such as cyclodextrins, pillar[5]arenes and calix[4]arenes into the POP-backbone have been shown to optimize properties of POPs for specific applications such as the removal of pollutants,[17,18] gas adsorption and separation,[19,20] sensing and catalysis.[21] The main motivation is to transfer the intrinsic properties of these cages/macrocycles in solution into the solid-state to achieve complex separations.

Cyclotetrabenzoin is a square-shaped macrocycle introduced by *Miljanić* and coworkers[22] as an excellent host for linear molecules such as CO_2, CS_2, organic nitriles, and terminal alkynes.[23,24] The cyclotetrabenzoin cavity is inaccessible to larger guest molecules such as *e.g.* CH_4, thus resulting in high CO_2/CH_4 selectivities.[24] Furthermore, this macrocycle can be readily functionalized by initial oxidation into an octaketone, and subsequent condensation reactions of these ketone moieties with aromatic *ortho*-diamines, which results in the formation of a three-dimensional structure through the distortion of the square-shaped cavity of cyclotetrabenzoin.[25] We recently demonstrated[7] a 3D macrocyclic POP containing cyclotetrabenzoin units, which showed a modest CO_2 uptake capacity along with an excellent CO_2/N_2 selectivity, by reacting the oxidized form of a cyclotetrabenzoin, namely octaketone (*Scheme 1*), with benzene-1,2,4,5-tetraamine hydrochloride under ionothermal conditions. However, this approach had limitations due to the rigidity of the polymeric structure and the abundance of mesopores, thus limiting the CO_2 uptake capacity.[26] In order to improve both CO_2 uptake capacity through higher nitrogen content and the higher abundance of micropores and ultramicropores, phenazine-2,3,7,8-tetraamine hydrochloride (PTAH) linker was introduced (*Scheme 1*). We also systematically investigated the effect of the reaction temperature on the textural properties of the polymers. Moreover, the traditional $ZnCl_2$/NaCl/KCl eutectic mixture was also replaced with a cheaper alternative, that is $AlCl_3$/NaCl eutectic molten salt mixture,[27,28] which was implemented as a reaction medium and a catalyst. The resulting 3D microporous macrocyclic POPs (3D-mmPOPs) showed surface areas up to 752 $m^2 g^{-1}$ with a micropore ratio of more than 90%, pore volumes up to 0.32 $cm^3 g^{-1}$ and enhanced CO_2 uptake capacity of 3.51 mmol g^{-1} at 273 K and 1.1 bar as well as a high CO_2 isosteric heat of adsorption, Q_{st}, of 40.6 kJ mol^{-1} at zero coverage originating from the presence of macrocyclic units.

Results and Discussion

The oxidation of cyclotetrabenzoin into the corresponding octaketone was carried out using nitric acid, as previously described (refer to the *Supporting Information* for detailed information).[25] The reaction between the octaketone and phenazine-2,3,7,8-tetraamine hydrochloride (PTAH) was conducted at three different temperatures, namely 200, 250 and 300 °C, utilizing an $AlCl_3$/NaCl eutectic salt mixture to prevent partial carbonization of the precursors and sublimation of $AlCl_3$ at elevated temperatures.[29,30] The formation of three-dimensional microporous organic polymers, 3D-mmPOPs, was verified by *Fourier* transform infrared (FT-IR) and X-ray photoelectron spectroscopy (XPS) analyses (*Figure 1*). A comparison of the 3D-mmPOPs synthesized at different temperatures was performed to better understand the impact of the reaction temperature on the chemical structure of the polymers. The octaketone exhibited distinct –C=O stretching bands appearing at 1691 and 1677 cm^{-1} (*Figure 1a* and *1b*).[7] These characteristic stretching bands disappeared after the polymerization reaction and new peaks at around 1604 cm^{-1} emerged in the FT-IR spectra of the 3D-mmPOPs, which can be attributed to the –C=N– stretching of pyrazines, indicating a successful polymerization reaction (*Figure 1a* and *1b*). Additionally, the characteristic –C–O bands of the octaketone at approximately 1205 and 1177 cm^{-1} disappeared, further supporting the formation of 3D-mmPOPs. Moreover, the typical –C=N– and –C=C– stretching bands of phenazine-2,3,7,8-tetraamine hydrochloride (PTAH) at *ca.* 1664, *ca.* 1620, and *ca.* 1491 cm^{-1} shifted to lower frequencies due to the polymerization.[31] Similarly, the –N–H vibrations of PTAH at *ca.* 3194 cm^{-1} disappeared in the spectra of 3D-mmPOP-250, but were observed as a shoulder in the 3D-mmPOP-200 spectra, indicating incomplete polymerization (*Figure 1a* and *1b*). The XPS survey spectra of the 3D-mmPOP-250 revealed the presence of carbon, nitrogen contents of 70.75, 9.4%, respec-

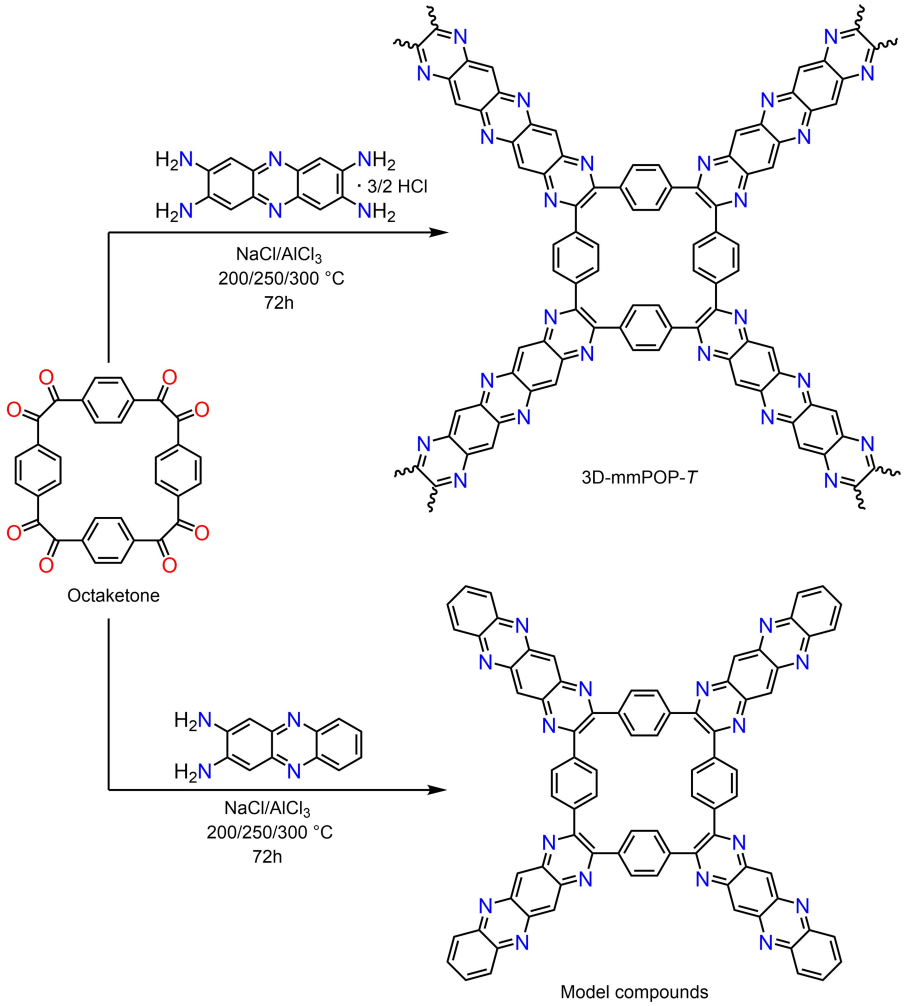

Scheme 1. Synthetic scheme and chemical structures of the 3D-mmPOP-*T*, model compounds, and octaketone. *T* represents the reaction temperature.

tively. We also observed the presence of oxygen atoms originating from terminal carbonyl moieties and aluminum oxide species along with trace amounts of other elements (*Figure S3*). The high-resolution C1s spectra exhibited peaks at 284.8, 286.4, 288.5, and 291.6 eV, which can be attributed to –C–C–/–C=C–, –C–N–/–C=N–, –C=O, and $\pi-\pi^*$ interactions, respectively (*Figure 1c*).[32,33] The presence of –C=O signals indicated the presence of end-groups and unreacted keto-groups. Additionally, the high-resolution N1s spectra revealed a single peak at 398.4 eV, corresponding to –C–N–/–C=N– and confirming the presence of only phenazine moieties.[28,32,33] The high-resolution O1s spectra showed peaks at 528.4 and 531.5 eV, which can be attributed to oxidized Indium from the support, varying aluminum oxide species and –C=O moieties.[32,34] Overall, the FT-IR and XPS spectra provide compelling evidence for the successful formation of 3D-mmPOPs and the presence of a small number of unreacted keto-groups.

To confirm the chemical structure of the 3D-mmPOPs, we also prepared the model compound using phenazine-2,3-diamine (named as model compound-*T*, where *T* is the reaction temperature) as shown in *Scheme 1*. The model compound synthesized at different temperatures was found to be entirely insoluble, necessitating the characterization through FT-IR spectroscopy (*Figure S5*). The FT-IR spectra displayed the disappearance of the ketone bands of octaketone (*ca.* 1691 and 1677 cm^{-1}) and amine stretching bands (*ca.* 3194 cm^{-1}) of phenazine-2,3-diamine in the spectra of the model compounds, signifying successful reaction completion (*Figure S5,a*). Furthermore, the characteristic –C=N– and –C=C–

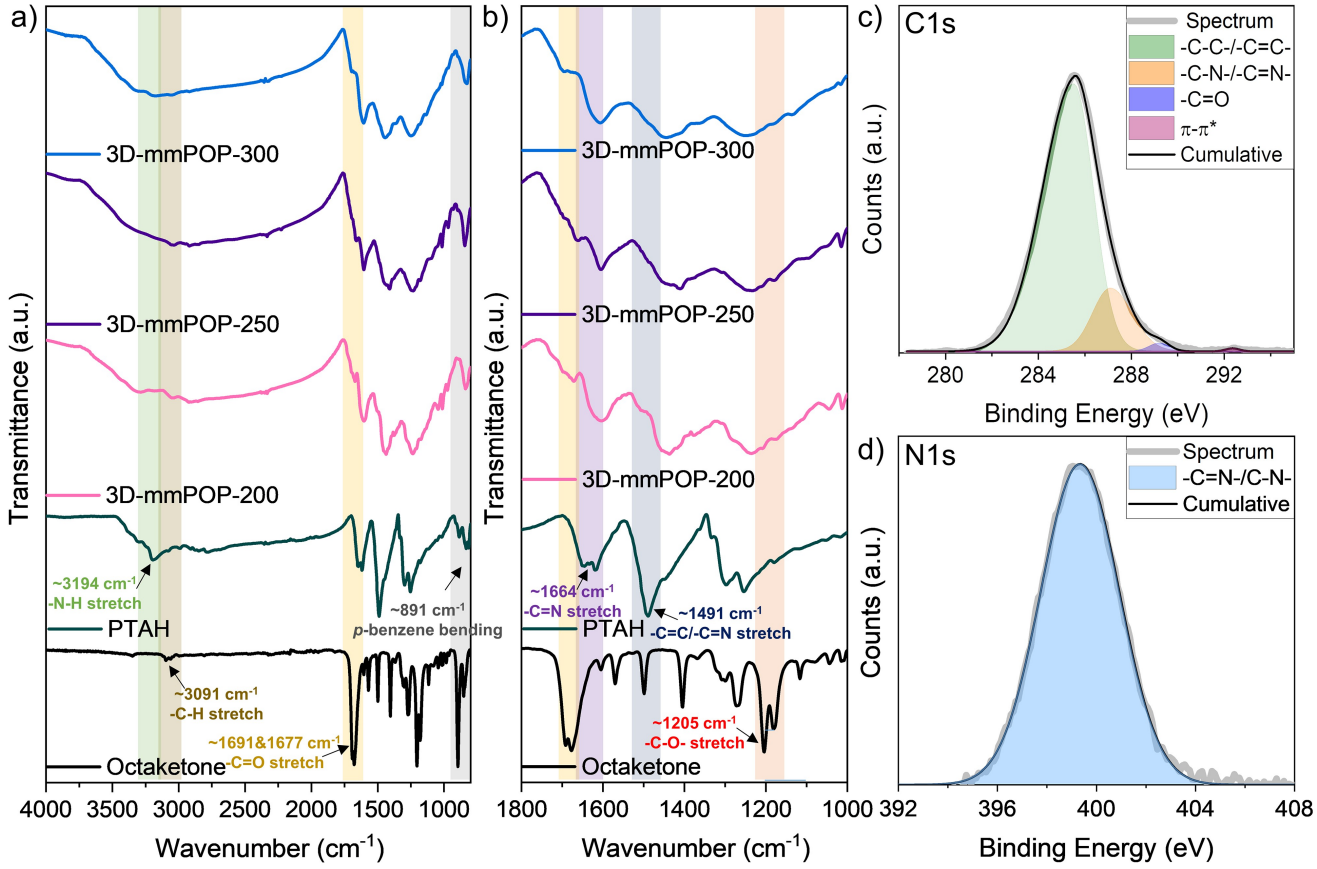

Figure 1. a) FT-IR spectra of the 3D-mmPOPs synthesized at different temperatures in comparison with the monomers; octaketone and PTAH. b) Expanded FT-IR region of 1000–1800 cm^{-1} to depict the C=O and C=N stretching bands. High-resolution C1s (c) and N1s (d) spectra of 3D-mmPOP-250.

bands of phenazine-2,3-diamine at *ca.* 1641 and 1490 cm^{-1}, respectively, exhibited a downward shift after the reaction (*Figure S5,b*), indicative of structural changes. To verify the structure of the model compounds, we conducted matrix-assisted laser desorption/ionization (MALDI) spectroscopy (*Figure S6*). The MALDI results confirmed the presence of the model compound synthesized at reaction temperatures of 200 and 250 °C. However, no model compound was detected in the reaction carried out at 300 °C, likely due to possible side reactions and carbonization.[26] This result underscores the need for careful temperature control in the synthesis. In order to further analyze the chemical structures of the 3D-mmPOPs and model compounds, ^{13}C cross-polarization magic angle spinning (CP-MAS) solid-state nuclear magnetic resonance (ssNMR) spectroscopy was employed (*Figure S7*). The ^{13}C-NMR spectra revealed two prominent peaks at 128.9 and 139.1 ppm, attributed to terminal carbons and –C=N– moieties, respectively.[7] Notably, an additional peak at 106.2 ppm was observed in the spectra of 3D-mmPOP-200, indicative of sp^2 carbon attached to amines, suggesting incomplete polymerization. Moreover, unreacted keto-groups at 178.1 ppm[7] were observed in the ^{13}C-NMR spectra of 3D-mmPOP-300 and Model compound-300, indicating the possibility of incomplete reaction. Furthermore, elemental analysis (EA) was performed to determine the elemental composition of the 3D-mmPOPs. The EA results showed similar carbon content in all the polymers, but the nitrogen content decreased with increasing reaction temperature (*Table S1*). Notably, 3D-mmPOP-200 exhibited higher nitrogen content (22.7%) compared to the theoretical value (19.4%), suggesting the presence of free amines due to incomplete polymerization. In contrast, 3D-mmPOP-300 displayed nitrogen content of less than half (9.3%) of the theoretical value (19.4%), likely due to partial carbonization and side reactions as also observed in the synthesis of model compound at this temperature.

3D-mmPOP-250 on the other hand demonstrated near-ideal nitrogen content of 18.8%. These EA results further corroborated the FT-IR and NMR findings, providing additional support for the characterization of the chemical structures of the 3D-mmPOPs and model compounds.

In order to assess the thermal stabilities of the 3D-mmPOPs, thermogravimetric analysis (TGA) was employed under both air and nitrogen atmospheres (*Figure S8*). The 3D-mmPOPs exhibited thermal stabilities up to 350 °C under nitrogen, except for 3D-mmPOP-200 displaying relatively lower stability, thus corroborating the findings from the FT-IR, EA and NMR spectra that suggested incomplete polymerization (*Figure S8a*). Intriguingly, TGA curves under air revealed some residual mass, possibly due to incomplete combustion[35] and partial presence of inorganic species and formation of carbonates that lead to a higher residual mass (*Figure S8b*). These findings collectively suggest that a reaction temperature of 200 °C is inadequate for efficient polymerization, resulting in the formation of oligomers. Conversely, a reaction temperature of 300 °C proves to be excessively high, leading to nitrogen loss due to side reactions and partial carbonization. Due to the residual mass found in the TGA measurements, we conducted inductively coupled plasma optical emission spectroscopy (ICP-OES) analyses of each sample to determine how much of the residual mass originates from residual aluminum chloride and its degradation products. The results (*Figure S9* and *Table S2*) confirmed a low Al content for mmPOP-250 of 2.31 wt% while mmPOP-200 and mmPOP-300 showed a residual Al content of 1.47 and 4.54 wt% respectively. The crystallinity of the 3D-mmPOPs was probed using X-ray diffraction (XRD) analysis, which showed amorphous structures, a common trait observed in POPs (*Figure S10*).[36]

The porosities of the 3D-mmPOPs were assessed through argon (Ar) adsorption-desorption analysis conducted at 77 K, as illustrated in *Figure 2a*. The surface area was calculated using the *Brunauer-Emmett-Teller* (BET) theory.[37] 3D-mmPOP-200 was found to be nonporous with a BET surface area of 4.7 $m^2 g^{-1}$, further corroborating the incomplete polymerization at this temperature (*Table S3*). Conversely, both 3D-mmPOP-250 and 3D-mmPOP-300 exhibited type 1 isotherms with surface areas of 751.9 and 678.3 $m^2 g^{-1}$, respectively, along with micropore ratios of 91% and 93% (S_{micro}/S_{total}) and pore volumes of 0.317 and 0.279 $cm^3 g^{-1}$, respectively (*Figure 3a* and *Table 1*).[38] Notably, both polymers displayed type I

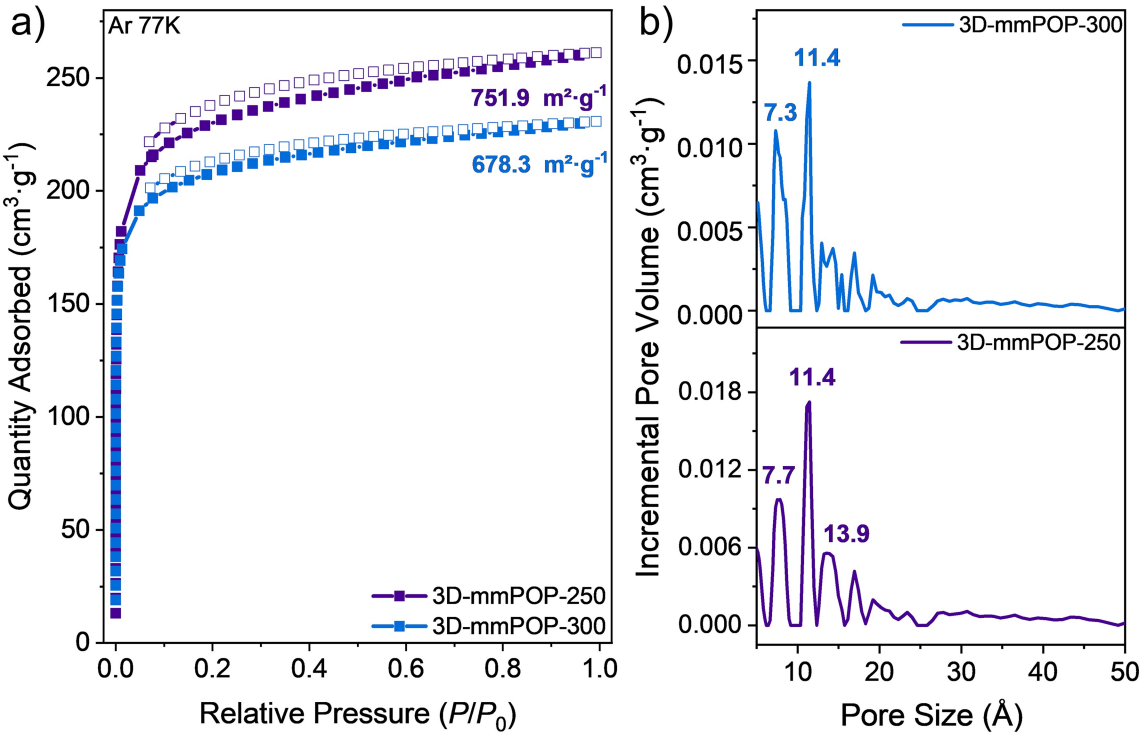

Figure 2. a) Ar uptake isotherms of 3D-mmPOPs measured at 77 K. Filled and empty symbols represent adsorption and desorption isotherms, respectively. b) Pore size distribution curves of 3D-mmPOP-250 and −300 obtained using NLDFT model.

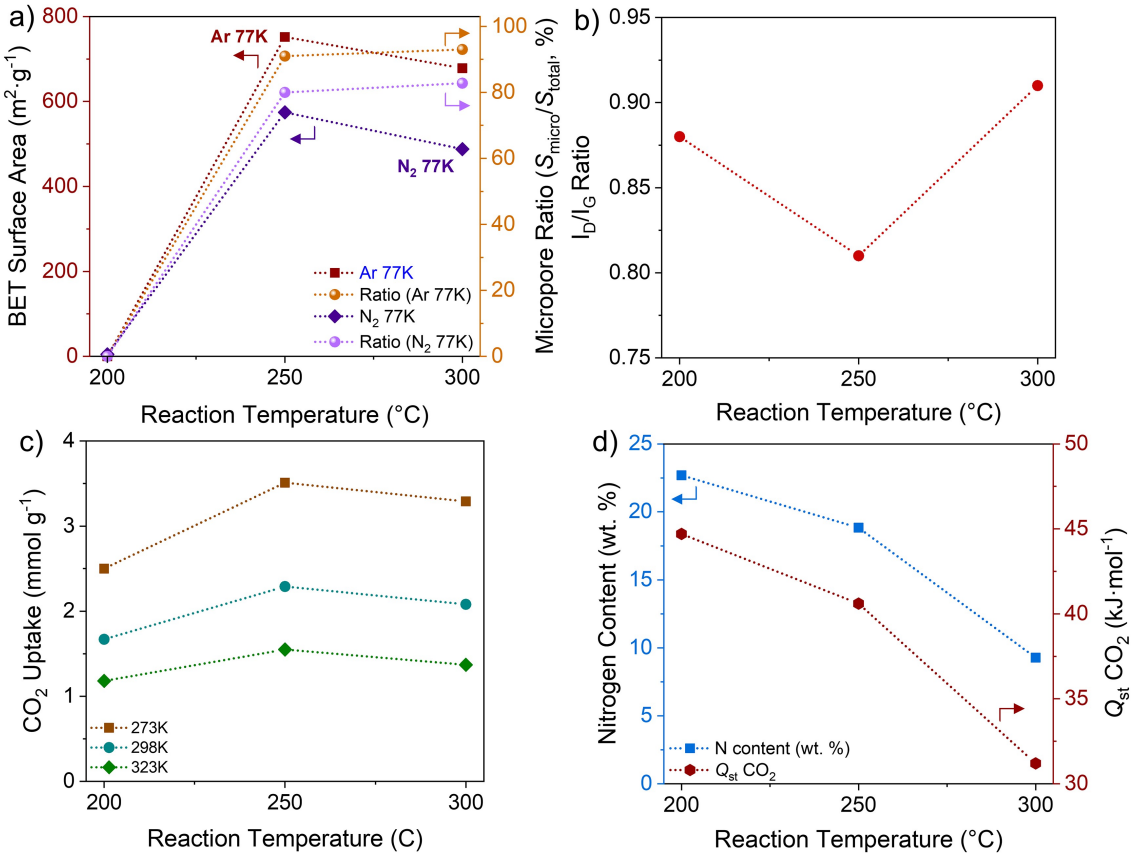

Figure 3. Change of the various properties of the 3D-mmPOPs *vs.* the reaction temperature: a) BET surface areas and micropore ratios, b) I_D/I_G ratio, c) CO_2 uptake capacities, d) heat of adsorption (Q_{st}) for CO_2 and nitrogen content.

Table 1. Porosity results of the 3D-mmPOPs obtained using Ar uptake at 77 K.

Sample	BET[a] [$m^2 g^{-1}$]	S_{micro}[b] [$m^2 g^{-1}$]	S_{ext}[c] [$m^2 g^{-1}$]	V_{total}[d] [$cm^3 g^{-1}$]	V_{micro}[e] [$cm^3 g^{-1}$]	V_{ext}[f] [$cm^3 g^{-1}$]
3D-mmPOP-250	751.9	681.2 (91 %)	70.7	0.317	0.252	0.065
3D-mmPOP-300	678.3	630.6 (93 %)	47.7	0.279	0.235	0.044

[a] BET surface area calculated over the pressure range (P/P_0) of 0.01 – 0.15. [b] Micropore surface area calculated using the *t*-plot method. [c] $S_{ext} = S_{total} - S_{micro}$. [d] Total pore volume obtained at $P/P_0 = 0.99$. [f] $V_{ext} = V_{total} - V_{micro}$.

isotherm, indicating highly microporous structures with no hysteresis.[39] It is noteworthy that although 3D-mmPOP-300 exhibited a lower BET surface area, the micropore ratio increased, possibly due to the partial carbonization, thus leading to pore fusing. To further elucidate the pore size characteristics of the 3D-mmPOPs, pore size distribution (PSD) analysis was conducted employing the nonlocal density functional theory (NLDFT) model.[40] The PSD curves unveiled the existence of pores with sizes of 7.7, 11.4, and 13.9 Å in 3D-mmPOP-250, with the 11.4 Å-sized pores exhibiting higher pore volumes (*Figure 2b*). In contrast, 3D-mmPOP-300 displayed pores with sizes of 7.3 and 11.4 Å in the PSD curve, again with 11.4 Å-sized pores having higher pore volumes (*Figure 2b*), which is consistent with the characterization results. We estimate that pores around *ca.* 7 Å belong to the square-shaped pore of the macrocycle and at 11.4 Å correspond to the larger cavity, respectively.[7] This can be seen better in the H4-type hysteresis of the POPs observed in the N_2 uptake measurements at 77 K, indicative of the presence of mesopores and slit-like pores (*Figures S11a* and *S11b*).

To gain further insights into the impact of carbonization at elevated temperatures, we conducted *Raman* spectroscopy on the 3D-mmPOPs, and scrutinized

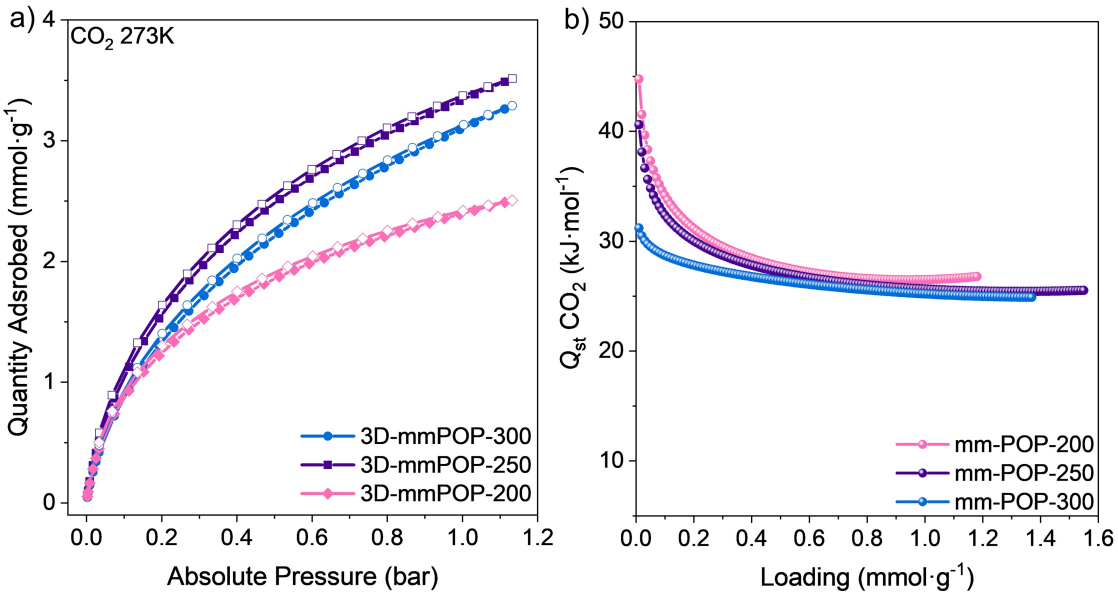

Figure 4. a) CO_2 uptake isotherms of 3D-mmPOPs measured at 273 K. Filled and empty symbols represent adsorption and desorption isotherms, respectively. b) Heat of adsorption (Q_{st}) for CO_2 of the 3D-mmPOPs.

the I_D/I_G ratios (*Figure S12*). The I_D/I_G ratio for 3D-mmPOP-200 was found to be 0.91, indicating a substantial presence of defects resulting from incomplete polymerization. Notably, this ratio decreased to 0.79 for 3D-mmPOP-250, indicating a reduction in defects (*Figure 3b*). However, the I_D/I_G ratio exhibited an increase to 0.87 for 3D-mmPOP-300, implying the formation of defects attributed to side reactions and partial carbonization. To unravel the morphology of the 3D-mmPOPs, we conducted Scanning Electron Microscopy (SEM) analysis (*Figure S13*). The SEM analysis revealed micron-sized particles with a rough surface observed at 200 °C, confirming the formation of oligomers. The effect of salt-templation was conspicuously evident at 300 °C, with cubical pores on the surface, suggestive of the disruption of the eutectic mixture due to water forming during the polycondensation reaction.[8] The *Raman* and SEM analyses corroborated the earlier findings and underscored 250 °C as the optimal reaction temperature for achieving a favorable combination of high surface area and low defect content.

The remarkable highly microporous structure exhibited by the 3D-mmPOPs prompted us to investigate their CO_2 uptake performance. Initially, we evaluated the CO_2 uptake capacities at 273 K (*Figure 4a*). Surprisingly, despite its nonporous nature, the 3D-mmPOP-200 displayed a noteworthy CO_2 uptake of 2.50 mmol g^{-1}, attributed to its high nitrogen content (*Table 2*). The highest CO_2 capture performance was achieved by 3D-mmPOP-250, with a remarkable uptake capacity of 3.51 mmol g^{-1}. Notably, although 3D-mmPOP-300 displayed a higher micropore content, its uptake capacity was slightly lower at 3.29 mmol g^{-1}, partially due to its lower nitrogen content (*Table 2*). The higher CO_2 uptake values compared to the earlier reported 3D-mPOP (2.29 mmol g^{-1})[7] was attributed to a higher nitrogen content as well as high microporosity and surface area. Moreover, using an extended linker, in the absence of interpenetration, leads to a better pore accessibility, which in return results in higher CO_2 uptake performance. We further investigated the CO_2 uptake performance at higher temperatures, specifically 298 and 323 K (*Figure S14*). As expected, the uptake values decreased with increasing temperature; however, even at these elevated temperatures, 3D-mmPOP-250 exhibited the highest capture performance, with uptake capacities of 2.29 mmol g^{-1} at 298 K and 1.55 mmol g^{-1} at 323 K, respectively

Table 2. CO_2 uptake at different temperatures and heat of adsorption for CO_2 results of 3D-mmPOPs.

Sample	CO_2 uptake [mmol g^{-1}]			Q_{st} [kJ mol^{-1}]
Temperature [K]	273	298	323	
3D-mmPOP-200	2.50	1.67	1.18	44.7–26.7
3D-mmPOP-250	3.51	2.29	1.55	40.6–25.5
3D-mmPOP-300	3.29	2.08	1.37	31.2–24.8

(*Table 2*). Notably, the trend of CO_2 uptake *vs.* reaction temperature closely paralleled that of BET surface area *vs.* reaction temperature (*Figure 3c*). Interestingly, with an uptake capacity of 3.51 mmol g^{-1} 3D-mmPOP-250 ranks among the best-performing macrocycle-based porous materials when compared to the literature (*Table S5*). To gain insights into the CO_2-philicity of the 3D-mmPOPs, we calculated the heat of adsorption (Q_{st}) for CO_2 by fitting the uptake isotherms obtained at 273 K, 298 K, and 323 K with a dual-site *Langmuir* model (*Figure S15* and *Table S4*).[41] Remarkably, 3D-mmPOP-200 exhibited the highest Q_{st} value of 44.7 kJ mol^{-1} at zero coverage, indicative of chemical binding, owing to the presence of free amines that facilitate strong CO_2 binding (*Figure 4b* and *Table 2*). Conversely, the Q_{st} results for 3D-mmPOP-250 exhibited the Q_{st} value of 40.6 kJ mol^{-1} at zero coverage, implying easier regeneration than sorbents based on chemisorption (*Figure 4b*).[42] Interestingly, the Q_{st} values for 3D-mmPOP-300 ranged from 31.2–24.8 kJ mol^{-1}, indicating purely physisorption, attributable to its lower nitrogen content (*Figure 4b*). This observation was further corroborated by plotting Q_{st} for CO_2 against nitrogen content, which revealed a similar decreasing trend with increasing reaction temperature (*Figure 3d*). The high Q_{st} values underscored the CO_2-philic nature of the 3D-mmPOPs, attributed to the presence of the CO_2-philic macrocycle. In summary, the CO_2 uptake values and heat of adsorption results collectively indicate that the reaction temperature of 250 °C leads to the formation of an optimal polymer structure with maximum CO_2 capture performance.

Conclusions

In conclusion, our study has successfully demonstrated the synthesis of fully sp^2-hybridized microporous 3D-POPs bearing macrocyclic units using $AlCl_3$/NaCl molten salt system. Furthermore, we have elucidated the significant impact of temperature on the polymeric network formation, enabling enhanced CO_2 uptake performance. Notably, by introducing an extended linker, we have improved upon our previously published macrocyclic POP, achieving a larger accessible surface area as well as higher nitrogen content. These findings highlight the potential of alternative cost-effective molten salt mixtures – beyond those containing $ZnCl_2$ – for the preparation of POPs. This research opens up new avenues for the development of advanced materials with enhanced CO_2 capture properties, paving the way for further advancements in sustainable energy and environmental applications.

Experimental Section

Materials and Methods

All the chemicals and solvents were used as purchased without any further purification. Solvents were purchased from *Fischer Chemicals*. Anhydrous $AlCl_3$ (98.5 %), NaCl (99.0 %), AcONa (99.0 %) were purchased from *Acros Organics*. HNO_3 solution (65 %) was purchased from *Fischer Chemicals* and benzene-1,2,4,5-tetraamine tetrahydrochloride (>95.0 %) was purchased from *Strem Chemicals*. All manipulations involving water and air-sensitive chemicals were carried in a glovebox under an Ar atmosphere. The degassing and reactions under inert atmosphere were carried out using standard *Schlenk* line techniques. FT-IR spectra were recorded on a *PerkinElmer Frontier* spectrometer using KBr pellets. XPS spectra were obtained on multipurpose XPS, *Sigma Probe*, *Thermo VG Scientific* by using Monochromatic Al Kα X-ray source. The samples were prepared on an indium foil to alleviate charging and enable the use of small sample amounts. The foil was supported on an aluminum foil and fixed on the XPS sample holder. High-resolution spectra were deconvoluted using fityk software.[43] TGA was performed on a *Mettler-Toledo TGA/DSC 3+* instrument using standard 70 μL alumina crucibles. The flow rate of the respective gas (air or N_2) was set to 20 sccm and the heating rate was set to 5 K/min. Inductively coupled plasma optical emission spectroscopy (ICP-OES) analyses were conducted on a *Perkin-Elmer Optima7000 DV*. Around 5 mg of sample were digested in 15 mL 5 % HNO_3 at 70 °C for 2 h. The samples were filtered using a 0.4 μm PTFE filter and directly measured. XRD patterns were acquired on STOE STADI-P system using Cu Kα1 incident beam using transmission mode. Samples were scanned between 2 and 60° of 2θ. Elemental analysis was carried out on a *ThermoFisher Flash 2000 CHNS* analyzer by using BBOT as a standard. *Raman* spectra were recorded on an *Alpha 300R Raman* microscope with a *UHTS 300* spectrometer using 535 nm laser excitation. SEM micrographs were recorded on *ThermoFisher Scios 2* instrument by using 3.0 kV accelerating voltage and 0.40 nA of current. Samples were pre-coated with 3.0 nm of gold layer on a *Cressington 208HR* sputtering tool prior to the SEM imaging. Liquid NMR spectra were recorded on *Bruker Avance III* 400 MHz spectrometer. The spectra were calibrated on the deuterated

solvent signal. Solid-state NMR spectra were recorded using *Bruker Avance Neo* 600 MHz instrument using 60.0 kHz spinning rates and 5.0 s of relaxation delay. The electrospray ionization mass spectrometry (ESI-MS) was performed on *Bruker Esquire HCT* instrument. HR-MALDI FT-ICR mass spectra were recorded on *Bruker FTMS 4.7T BioAPEX II* in positive mode using *trans*-2-[3-(*tert*-butylphenyl)-2-methyl-2-propenylidene]malononitrile (DCTB) as a matrix and sodium trifluoroacetate (NaTFA) as the counter ion source.[44] The N_2, Ar and CO_2 adsorption isotherms were obtained on *Micromeritics 3Flex* instrument at respective temperatures. The samples were degassed at 120 °C under vacuum for 12 h prior to the measurements.

Synthesis of the POPs

Synthesis of the POPs were performed by following our earlier reported procedures.[27,28] A *Pyrex* ampule was charged with powdered NaCl (82.4 mg, 1.41 mmol, 7.04 equiv.), octaketone (106.5. mg, 0.2 mmol, 1.00 equiv.) and PTAH (118 mg, 0,4 mmol, 2 equiv.) before being transferred into the glovebox, where $AlCl_3$ (298.7 mg, 2.24 mmol, 11.2 equiv.) was added. The contents of the ampule were evacuated for 45 min to an internal pressure of 0.15 mbar and flame-sealed. The contents of the ampule were heated at respective temperatures for 72 h. After cooling to room temperature, the obtained black solid was stirred in a 1 : 1 mixture of water and methanol for 72 h. The solids were isolated by filtration using a *POR4* fritted glass filter and washed with water, methanol, tetrahydrofuran and acetone before being stirred in deionized water overnight. Finally, polymers were purified by *Soxhlet* extraction using methanol for 24 h and dried at 90 °C under a vacuum to yield 120.3 mg (69.4 %) of 3D-mmPOP-200, 134.1 mg (77.4 %) of 3D-mmPOP-250, and 132.7 mg (76.6 %) of 3D-mmPOP-300 as black powders.

The model compounds were synthesized using the exact same procedures with phenazine-2,3-diamine.

Acknowledgements

The authors would like to express our gratitude to the following funding agencies and individuals for their generous support in making this research possible. Prof. *Ali Coskun* acknowledges the Swiss National Science Foundation (SNF) for their funding through grant 200021-175947. Prof. *Ognjen Miljanić* extends his thanks to the donors of the American Chemical Society Petroleum Research Fund for their support through grant ND-58919, as well as the Welch Foundation for grant E1768, and the US National Science Foundation for grant CHE-2204236. Open Access funding provided by Université de Fribourg.

Data Availability Statement

The data that support the findings of this study are openly available in Zenodo at https://doi.org/10.5281/zenodo. 8061203.

Author Contribution Statement

T. A. performed the synthesis of the polymers. *T. P.* and *A. R.* performed the synthesis of the octaketone. *P. W. F.* helped with the analysis of the polymers and synthesized the precursors. *K. P.* helped with NMR measurements. *A. C.* and *O. Š. M.* procured funds, conceived and supervised the project, and wrote the manuscript together with all other authors.

References

[1] N. O. A. Administration, https://gml.noaa.gov/ccgg/trends/monthly.html, 2023.
[2] S. Solomon, G.-K. Plattner, R. Knutti, P. Friedlingstein, 'Irreversible climate change due to carbon dioxide emissions', *Proc. Natl. Acad. Sci. U.S.A.* **2009**, *106*, 1704–1709.
[3] K. S. Song, P. W. Fritz, A. Coskun, 'Porous organic polymers for CO_2 capture, separation and conversion', *Chem. Soc. Rev.* **2022**, *51*, 9831–9852.
[4] P. Bhanja, A. Modak, A. Bhaumik, 'Porous Organic Polymers for CO_2 Storage and Conversion Reactions', *ChemCatChem* **2019**, *11*, 244–257.
[5] A. K. Sekizkardes, P. Wang, J. Hoffman, S. Budhathoki, D. Hopkinson, 'Amine-functionalized porous organic polymers for carbon dioxide capture', *Mater Adv* **2022**, *3*, 6668–6686.
[6] Y. Zhu, H. Long, W. Zhang, 'Imine-Linked Porous Polymer Frameworks with High Small Gas (H_2, CO_2, CH_4, C_2H_2) Uptake and CO_2/N_2 Selectivity', *Chem. Mater.* **2013**, *25*, 1630–1635.
[7] T. Ashirov, M. Alrayyani, K.-S. Song, O. Š. Miljanić, A. Coskun, 'Cyclotetrabenzil-Based Porous Organic Polymers with High Carbon Dioxide Affinity', *Org. Mater.* **2021**, *03*, 346–352.
[8] T. Ashirov, K. S. Song, A. Coskun, 'Salt-Templated Solvothermal Synthesis of Dioxane-Linked Three-Dimensional Nanoporous Organic Polymers for Carbon Dioxide and Iodine Capture', *ACS Appl. Nano Mater.* **2022**, *5*, 13711–13719.

[9] V. Rozyyev, M. S. Yavuz, D. Thirion, T. S. Nguyen, T. P. N. Nguyen, A.-H. Emwas, C. T. Yavuz, 'Optimizing bromide anchors for easy tethering of amines, nitriles and thiols in porous organic polymers towards enhanced CO_2 capture', *Microporous Mesoporous Mater.* **2021**, *328*, 111450.

[10] K. S. Song, S. N. Talapaneni, T. Ashirov, A. Coskun, 'Molten Salt Templated Synthesis of Covalent Isocyanurate Frameworks with Tunable Morphology and High CO_2 Uptake Capacity', *ACS Appl. Mater. Interfaces* **2021**, *13*, 26102–26108.

[11] M. M. Abdelnaby, T. A. Saleh, M. Zeama, M. A. Abdalla, H. M. Ahmed, M. A. Habib, 'Azo-Linked Porous Organic Polymers for Selective Carbon Dioxide Capture and Metal Ion Removal', *ACS Omega* **2022**, *7*, 14535–14543.

[12] O. M. El-Kadri, T.-D. Tessema, R. M. Almotawa, R. K. Arvapally, M. H. Al-Sayah, M. A. Omary, H. M. El-Kaderi, 'Pyrene Bearing Azo-Functionalized Porous Nanofibers for CO_2 Separation and Toxic Metal Cation Sensing', *ACS Omega* **2018**, *3*, 15510–15518.

[13] H. A. Patel, J. Byun, C. T. Yavuz, 'Carbon Dioxide Capture Adsorbents: Chemistry and Methods', *ChemSusChem* **2017**, *10*, 1303–1317.

[14] X. Yang, Z. Ullah, J. F. Stoddart, C. T. Yavuz, 'Porous Organic Cages', *Chem. Rev.* **2023**, *123*, 4602–4634.

[15] C.-Y. Yao, A. P. de Silva, 'Recent developments in CO_2 capture/storage/utilization with aromatic macrocycles', *Carbon Capture Sci. Technol.* **2022**, *4*, 100058.

[16] O. Buyukcakir, Y. Seo, A. Coskun, 'Thinking Outside the Cage: Controlling the Extrinsic Porosity and Gas Uptake Properties of Shape-Persistent Molecular Cages in Nanoporous Polymers', *Chem. Mater.* **2015**, *27*, 4149–4155.

[17] T. Skorjanc, D. Shetty, A. Trabolsi, 'Pollutant removal with organic macrocycle-based covalent organic polymers and frameworks', *Chem* **2021**, *7*, 882–918.

[18] D. Shetty, J. Raya, D. S. Han, Z. Asfari, J.-C. Olsen, A. Trabolsi, 'Lithiated Polycalix[4]arenes for Efficient Adsorption of Iodine from Solution and Vapor Phases', *Chem. Mater.* **2017**, *29*, 8968–8972.

[19] W. Chen, P. Chen, G. Zhang, G. Xing, Y. Feng, Y.-W. Yang, L. Chen, 'Macrocycle-derived hierarchical porous organic polymers: synthesis and applications', *Chem. Soc. Rev.* **2021**, *50*, 11684–11714.

[20] S. N. Talapaneni, D. Kim, G. Barin, O. Buyukcakir, S. H. Je, A. Coskun, 'Pillar[5]arene Based Conjugated Microporous Polymers for Propane/Methane Separation through Host–Guest Complexation', *Chem. Mater.* **2016**, *28*, 4460–4466.

[21] Z. Li, Y.-W. Yang, 'Macrocycle-Based Porous Organic Polymers for Separation, Sensing, and Catalysis', *Adv. Mater.* **2022**, *34*, 2107401.

[22] Q. Ji, H. T. M. Le, X. Wang, Y.-S. Chen, T. Makarenko, A. J. Jacobson, O. Š. Miljanić, 'Cyclotetrabenzoin: Facile Synthesis of a Shape-Persistent Molecular Square and Its Assembly into Hydrogen-Bonded Nanotubes', *Chem. Eur. J.* **2015**, *21*, 17205–17209.

[23] A. M. Eisterhold, T. Puangsamlee, S. Otterbach, S. Bräse, P. Weis, X. Wang, K. V. Kutonova, O. Š. Miljanić, 'Expanded Cyclotetrabenzoins', *Org. Lett.* **2021**, *23*, 781–785.

[24] Y.-T. Wang, C. McHale, X. Wang, C.-K. Chang, Y.-C. Chuang, W. Kaveevivitchai, O. Š. Miljanić, T.-H. Chen, 'Cyclotetrabenzoin Acetate: A Macrocyclic Porous Molecular Crystal for CO_2 Separations by Pressure Swing Adsorption', *Angew. Chem. Int. Ed.* **2021**, *60*, 14931–14937.

[25] S. Hahn, M. Alrayyani, A. Sontheim, X. Wang, F. Rominger, O. Š. Miljanić, U. H. F. Bunz, 'Synthesis and Characterization of Heterobenzenacyclo-octaphanes Derived from Cyclotetrabenzoin', *Chem. Eur. J.* **2017**, *23*, 10543–10550.

[26] J. Maschita, T. Banerjee, G. Savasci, F. Haase, C. Ochsenfeld, B. V. Lotsch, 'Ionothermal Synthesis of Imide-Linked Covalent Organic Frameworks', *Angew. Chem. Int. Ed.* **2020**, *59*, 15750–15758.

[27] P. W. Fritz, T. Chen, T. Ashirov, A.-D. Nguyen, M. Dincă, A. Coskun, 'Fully Conjugated Tetraoxa[8]circulene-Based Porous Semiconducting Polymers', *Angew. Chem. Int. Ed.* **2022**, *61*, e202116527.

[28] K. Kim, S. Kim, S. N. Talapaneni, O. Buyukcakir, A. M. I. Almutawa, K. Polychronopoulou, A. Coskun, 'Transition metal complex directed synthesis of porous cationic polymers for efficient CO_2 capture and conversion', *Polymer* **2017**, *126*, 296–302.

[29] K. S. Mohandas, N. Sanil, T. Mathews, P. Rodriguez, 'An electrochemical investigation of the thermodynamic properties of the NaCl–$AlCl_3$ system at subliquidus temperatures', *Metall. Mater. Trans. B* **2001**, *32*, 669–677.

[30] C. Robelin, P. Chartrand, A. D. Pelton, 'Thermodynamic evaluation and optimization of the (NaCl + KCl + $AlCl_3$) system', *J. Chem. Thermodyn.* **2004**, *36*, 683–699.

[31] C. Stammer, A. Taurins, 'Infrared spectra of phenazines', *Spectrochim. Acta* **1963**, *19*, 1625–1654.

[32] J. F. Moulder, W. F. Stickle, P. S. Sobol, K. D. Bomben, 'Handbook of X-ray Photoelectron Spectroscopy: A Reference Book of Standard Spectra for Identification and Interpretation of XPS Data', Eds. J. Chastain, R. C. King, Physical Electronics Division, Perkin-Elmer Corp., Eden Prairie, Minnesota, **1995**.

[33] T. Ashirov, J. S. Siena, M. Zhang, A. Ozgur Yazaydin, M. Antonietti, A. Coskun, 'Fast light-switchable polymeric carbon nitride membranes for tunable gas separation', *Nat. Commun.* **2022**, *13*, 7299.

[34] J.-C. Dupin, D. Gonbeau, P. Vinatier, A. Levasseur, 'Systematic XPS studies of metal oxides, hydroxides and peroxides', *Phys. Chem. Chem. Phys.* **2000**, *2*, 1319–1324.

[35] M. d. F. Salgado, A. M. Abioye, M. M. Junoh, J. A. P. Santos, F. N. Ani, 'Preparation of activated carbon from babassu endocarpunder microwave radiation by physical activation', *IOP Conf. Ser.: Earth Environ. Sci.* **2018**, *105*, 012116.

[36] H. Bildirir, V. G. Gregoriou, A. Avgeropoulos, U. Scherf, C. L. Chochos, 'Porous organic polymers as emerging new materials for organic photovoltaic applications: current status and future challenges', *Mater. Horiz.* **2017**, *4*, 546–556.

[37] S. Brunauer, P. H. Emmett, E. Teller, 'Adsorption of Gases in Multimolecular Layers', *J. Am. Chem. Soc.* **1938**, *60*, 309–319.

[38] M. Thommes, K. Kaneko, A. V. Neimark, J. P. Olivier, F. Rodriguez-Reinoso, J. Rouquerol, K. S. W. Sing, 'Physisorption of gases, with special reference to the evaluation of surface area and pore size distribution (IUPAC Technical Report)', *Pure Appl. Chem.* **2015**, *87*, 1051–1069.

[39] F. J. Sotomayor, K. A. Cychosz, M. Thommes, 'Characterization of Micro/Mesoporous Materials by Physisorption:

Concepts and Case Studies', *Acc. Mater. Surf. Res.* **2018**, *3*, 34–50.
[40] G. Kupgan, T. P. Liyana-Arachchi, C. M. Colina, 'NLDFT Pore Size Distribution in Amorphous Microporous Materials', *Langmuir* **2017**, *33*, 11138–11145.
[41] I. Langmuir, 'The Adsorption of Gases on Plane Surfaces of Glass, Mica and Platinum', *J. Am. Chem. Soc.* **1918**, *40*, 1361–1403.
[42] R. Dawson, D. J. Adams, A. I. Cooper, 'Chemical tuning of CO_2 sorption in robust nanoporous organic polymers', *Chem. Sci.* **2011**, *2*, 1173–1177.
[43] M. Wojdyr, '*Fityk*: a general-purpose peak fitting program', *J. Appl. Crystallogr.* **2010**, *43*, 1126–1128.
[44] I. Mandal, A. Mandal, M. A. Rahman, A. F. M. Kilbinger, 'Chain transfer agents for the catalytic ring opening metathesis polymerization of norbornenes', *Chem. Sci.* **2022**, *13*, 12469–12478.

Received May 10, 2023
Accepted June 20, 2023

